

NONLINEAR LATERAL RESPONSE OF PILE GROUP IN CLAY USING THE MODIFIED CAM CLAY SOIL MODEL

Avinash V Navale¹, Chandresh H Solanki¹, Vishwas A Sawant^{2*} , Yamini Jala²

¹Sardar Vallabhbhai National Institute of Technology Surat, Surat, 395007 Gujarat, India

²Indian Institute of Technology Roorkee, Roorkee, 247667 Uttarakhand, India

Date received: 15/08/2022 Date accepted: 11/01/2023

*Corresponding author's email: vishwas.sawant@ce.iitr.ac.in

DOI: 10.33736/jcest.4909.2023

Abstract – Lateral pile response of the 3×3 square pile group has been investigated in terms of lateral displacement and maximum bending moment using three-dimensional finite element analysis. Soil is represented using 8-node isoparametric elements. Piles and pile cap are modelled using 20-node isoparametric elements. The 16-node isoparametric interface elements are used to establish the continuity between the pile and surrounding soil. Soil is represented by the modified Cam clay criterion. The entire code has been developed in FORTRAN 90. The parametric study has been performed to investigate the effect of yield criteria, soil modulus, pile spacing, pile diameter and pile length-to-diameter ratio on the response of the 3×3 pile group embedded in clay. A considerable effect of these parameters is observed. It is found that the maximum bending moment in the middle row of the pile group is higher than the front and rear rows for all cases considered in the study. The pile displacement and bending moments in the pile group reduce with an increase in soil modulus, pile spacing and pile diameter. As pile slenderness is increased, it causes an increase in displacement of the pile and a decrease in the maximum bending moment. The modified Cam clay model predicts greater displacements as compared to the Mohr-Coulomb model highlighting the impact of p_0 on the yield surface. From the results obtained, the ultimate loads are predicted at a displacement of 5 mm, 10 % of diameter and 20% of diameter.

Copyright © 2023 UNIMAS Publisher. This is an open access article distributed under the Creative Commons Attribution-NonCommercial-ShareAlike 4.0 International License which permits unrestricted use, distribution, and reproduction in any medium, provided the original work is properly cited.

Keywords: Lateral displacement, pile spacing, modified Cam clay model, pile group, ultimate load

1.0 INTRODUCTION

Structures like offshore platforms, wind turbines, multistoried buildings, transmission towers, etc. are subjected to heavy lateral loads due to waves, wind and earthquakes. Due to nature and amount of load and the prevailing soil conditions, pile foundations are the obvious choice in most situations. Generally, piles are used in groups. The problem of the laterally loaded pile in the horizontal ground was addressed by many researchers way back from Reese and Matlock [1]. Analytical, numerical and experimental studies are reported to predict pile response.

For short (rigid) piles, formulas proposed by Broms [2] are used to estimate the ultimate load. For long (flexible) piles, three approaches have been widely used depending on the representation of soil media. Subgrade reaction (p - y) approach is used, in which soil is represented by a number of closely spaced independent springs. The soil reaction at a point is proportional to pile displacement at a given point. In the elastic continuum approach, the soil is considered an elastic continuum and the pile is assumed as an infinitely thin elastic strip embedded in soil media. Pile and soil displacements are equated at nodal points. In the finite element method, both pile and soil are considered as a continuum using a number of elements. The soil domain is to be modeled to be up to a suitable distance.

Sogge [3] analysed the laterally loaded pile behaviour using the finite element method. The pile was modelled using beam elements whereas the surrounding soil was modelled as Winkler springs using linear subgrade reaction modulus. Rajashree and Sundaravadivelu [4] proposed a hyperbolic p - y relationship based on the undrained shear strength and the modulus of subgrade reaction for laterally loaded piles in soft clay. Pile was idealized as the beam element and the soil was represented by elasto-plastic sub-elements considering non-linear inelastic spring elements. Desai and Appel [5] have presented a three-dimensional elastic finite element analysis of laterally loaded piles, using eight-node hexahedral continuum elements and eight-node interface elements. Solutions to this type of problem have also been obtained by using two-dimensional finite element analysis [6, 7]. Linear strain triangles in the semi-analytical finite element formulation were used by Randolph [8]. Results were fitted by algebraic

expressions, from which the lateral response of a single pile was readily calculated. Al-Khazaali and Vanapalli [9] highlighted the impact of capillary suction in load distribution characteristic of different piles. Finite element analysis, using PLAXIS 2D software was conducted to calculate the load distribution plot of model piles software. A three-dimensional coupled finite element algorithm was developed by Damluji and Anbanki [10] to predict the behaviour of single pile in clay. Each node of the 20 node brick element had four degrees of freedom, three for displacements and one for pore water pressure. The pile behaviour was modeled through linear elastic constitutive relationship while that of soil by Modified Cam Clay model. The load displacement results and built of pore water pressure and their dissipation showed good agreement with experimental studies. Simplified finite element analysis was proposed by Desai et al. [11] for analysis of pile group. Beam-column, plate and non-linear spring elements were used for simulating piles, cap and foundations respectively [12]. Zaman et al. [13] used a non-linear 3D finite element method in order to explore the effects of pile-cap thickness and pile inclination when the several forces like axial and shear force, battered pile in a group and a group consisting of vertical and batter piles. Concrete damaged plasticity model and anisotropic modified Cam Clay model were used to represent the behavior of pile and soil respectively. From the study it was found that the largest resistance was offered by battered pile group and least was offered by vertical pile group. The ultimate lateral resistance of the piles in cohesive soil was studied by Hazzar et al. [14] using FLAC 2D software. The reliability of Brom's method was verified and the effects of factors such as pile diameter, pile length, axial load and clay stiffness were studied. Ilyas et al. [15] performed centrifuge model tests to investigate the behavior of laterally pile groups in normally consolidated and overconsolidated kaolin clay. Group efficiency falls as the number of piles in a group grows for both NC and OC clay pile groups with a center-to-center pile spacing of $3D$ (where D is the pile diameter). However, when the pile separation is increased to $5D$, the group interaction effect becomes minimal. Chandrasekaran et al. [16] conducted lateral load tests on pile group consisting of model piles in soft clay and reported the results. The configurations considered were 1×2 , 2×2 , 1×4 , and 3×3 model pile groups. Results indicated that there was considerable difference in the p -multipliers in the row of linear arrangement and stresses, displacement and bending moments were distributed in different piles in a group. Dewaikar et al. [17] presented nonlinear 3-D finite element analysis incorporating the no tension behaviour, gapping in the soil pile contact and yielding of the soil. The soil was modelled using the von Mises yield criteria and pile was treated linear elastic. 20 node isoparametric continuum elements were used to model the soil and pile; the pile soil contact was modelled using the 8node interface element. Karthigeyan et al. [18] investigated the lateral response of piles under the influence of vertical loads installed in sandy soils through 3-D finite element analyses. The Drucker-Prager constitutive model with non-associated flow rule was used for sandy soils. Farsakh et al. [19] compared the static lateral load behaviour of a vertical pile group, by the same row in square arrangement. Halder and Halder and Bandyopadhyay [20] considered laterally loaded piles in clay having different properties along depth, OASYS Alp 19.2 software was used for study. The findings revealed that design of laterally loaded pile is economical if plastic analysis is used. Yu et al. [21] carried out assessment of six existing initial stiffness models. He carried out comparison from robust design point of view. Multiple objectives such as safety, cost and design robustness were considered. The best initial stiffness model for laterally loaded pile design was suggested and simplified. Li et al. [22] developed a 3D pile element model which can simulate the pile behavior under complex loading in 3D space. Soils were not modeled explicitly as direct integration of soil properties into element formulation was carried out. Luo et al. [23] investigated the limiting force profile (LFP) for laterally loaded piles embedded in undrained clay. Empirical formula for flow around condition and a generic design model and procedure for determination of model parameters to determine the limiting soil resistance under wedge failure is proposed.

Subgrade reaction (p - y curve) approach is most popular. p - y reaction curves that relate the horizontal displacement of the pile (y), in each layer of soil, to the soil reaction (p) exerted by the soil [1]. p -multiplier, a constant used to modify p - y curves for an isolated single pile, is a convenient way to express the loss in soil resistance due to group effect. However, to model continuity of soil, nonlinearity of soil, behavior at pile-soil interface, complex boundary conditions, layered soil and heterogeneous material properties, finite element analysis as the best alternative. From the literature review, it is observed that though finite element method has been used by many researchers, the use of critical state models to represent soil is limited.

In the present study, the analysis of 3×3 pile group subjected to lateral load is carried out using 3D finite element analysis. The nonlinear behavior of soil is modeled by modified Cam clay criterion. Computer program is developed in FORTRAN 90. The linear elastic model is insufficient to capture the essential features of soil. Stress states in the linear elastic model are not limited in any way, which means that the model shows infinite strength. Mohr-Coulomb model does not include stress dependency, stress-path dependency, strain dependency of stiffness, or anisotropic stiffness although the increase in stiffness with depth can be considered. This model does not

automatically include the increase in shear strength with consolidation when modelled for undrained material. Modified Cam clay model accounts for isotropic volume changes associated with actual all-round stress p acting on the soil element. Shape and extent of yield surface is also function of stress ratio p/p_0 . Model can incorporate appropriate hardening softening behaviour based on stress levels.

2.0 PROBLEM DEFINITION

Piles are assumed to remain in elastic state during entire analysis and nonlinear behavior of soil is modeled by modified Cam clay criterion. Piles, pile cap and soil are represented by isoparametric continuum elements. As piles and pile cap are subjected to bending, twenty node continuum elements having quadratic shape functions are used to model them. As soil is subjected to shear, eight node continuum elements having linear shape functions are used to model it. Sixteen node interface elements are used to model pile soil interface. High normal stiffness and less tangential stiffness of interface elements is assumed to prohibit gapping and allow only slipping between pile and soil.

2.1. Elasto-Plastic Behaviour

Pile is modelled as elastic material whereas soil is modelled as elasto plastic material. Plasticity theory with elasto-plastic constitutive laws is used to model the soil behaviour after yielding. A yield functions is defined which separates purely elastic state from elasto-plastic state. A plastic potential function specifies the direction of plastic straining at every stress state after yielding by means of a flow rule. A hardening/softening rule prescribes how yield function varies with the plastic strains.

The simple elasto-plastic models have certain limitations. Some basic features after yielding like hardening and softening can't be modelled. Also, if same yield function and plastic potential function (associative flow rule) are used, they predict excessive dilatancy during yielding. Hence one of the critical state models, modified Cam clay model is used in this study.

In general yield functions are expressed in terms of stress invariants; mean effective stress, p' , deviatoric stress J and Lode's angle θ . They are related with principal stresses with following relationship [24].

$$p' = \frac{\sigma_1 + \sigma_2 + \sigma_3}{3} \quad J = \frac{1}{\sqrt{6}} \sqrt{(\sigma_1 - \sigma_2)^2 + (\sigma_2 - \sigma_3)^2 + (\sigma_3 - \sigma_1)^2} \quad (1)$$

$$\text{and } \theta = \tan^{-1} \left(\frac{1}{\sqrt{3}} \left(2 \frac{(\sigma_2 - \sigma_3)}{(\sigma_1 - \sigma_3)} - 1 \right) \right)$$

In elasto-plastic state, incremental stresses, $\{\Delta\sigma\}$ and incremental strains $\{\Delta\varepsilon\}$ are related with each other as given in equation below.

$$\{\Delta\sigma\} = [D]_{ep} \{\Delta\varepsilon\} \quad (2)$$

where, $[D]_{ep}$ is elasto-plastic constitutive matrix. $[D]_{ep}$ is correlated with elastic constitutive matrix $[D]$, plastic potential function P and yield function F through following relationship.

$$[D]_{ep} = [D] - \frac{[D] \left\{ \frac{\partial P}{\partial \sigma} \right\} \left\{ \frac{\partial F}{\partial \sigma} \right\}^T [D]}{A + \left\{ \frac{\partial F}{\partial \sigma} \right\}^T [D] \left\{ \frac{\partial P}{\partial \sigma} \right\}} \quad (3)$$

A is hardening parameter. For material with perfect plasticity, $A = 0$ [24].

Using chain rule, the flow vector, $a = \{\partial F / \partial \sigma\}$, can be written as:

$$a = \frac{\partial F}{\partial \sigma} = \frac{\partial F}{\partial p'} \frac{\partial p'}{\partial \sigma} + \frac{\partial F}{\partial J} \frac{\partial J}{\partial \sigma} + \frac{\partial F}{\partial \theta} \frac{\partial \theta}{\partial \sigma} \quad (4)$$

It can also be expressed as explained by Nayak and Zienkiwicz [25]

$$a = C_1 a_1 + C_2 a_2 + C_3 a_3 \quad (5)$$

where, $C_1 = \frac{\partial F}{\partial p'}$; $C_2 = \frac{\partial F}{\partial J}$; $C_3 = \frac{\partial F}{\partial \theta}$ and $a_1 = \frac{\partial p'}{\partial \sigma}$; $a_2 = \frac{\partial J}{\partial \sigma}$; $a_3 = \frac{\partial \theta}{\partial \sigma}$

$$a_1 = \frac{\partial p'}{\partial \sigma} = \frac{1}{3} [1 \ 1 \ 1 \ 0 \ 0 \ 0]^T$$

$$a_2 = \frac{\partial J}{\partial \sigma} = \frac{1}{2J} [\sigma_x - p' \ \sigma_y - p' \ \sigma_z - p' \ 2\tau_{xy} \ 2\tau_{yz} \ 2\tau_{zx}]^T$$

$$a_3 = \frac{\partial \theta}{\partial \sigma} = \frac{\sqrt{3}}{2J^3 \cos 3\theta} \left(3 \frac{J_3}{J} \frac{\partial J}{\partial \sigma} - \frac{\partial J_3}{\partial \sigma} \right) \quad (6)$$

where, $J_3 = \begin{vmatrix} \sigma_x - p' & \tau_{xy} & \tau_{zx} \\ \tau_{xy} & \sigma_y - p' & \tau_{yz} \\ \tau_{zx} & \tau_{yz} & \sigma_z - p' \end{vmatrix}$

2.2. Modified Cam Clay Model

It is assumed that during drained isotropic compression, moves along a trajectory in $v - \ln p'$ plane, which consists of a virgin consolidation line and set of swelling lines. Virgin consolidation line are assumed to be straight in $v - \ln p'$ space governed by equation $v - \lambda \ln p' = v_1$. Similarly swelling lines follow equation $v - \kappa \ln p' = v_s$. The values of λ , κ and v_1 are characteristics of particular type clay. v_s is different for each swelling line. Bulk modulus of soil can be related with the slope of swelling line.

$$K = \frac{d p'}{d \varepsilon_v^e} = \frac{v p'}{\kappa} \quad (7)$$

The yield function of modified Cam clay model can be expressed in terms of stress invariants as,

$$\left(\frac{J}{p' g(\theta)} \right)^2 - \left(\frac{p_0}{p'} - 1 \right) = 0 \quad \text{where} \quad g(\theta) = \frac{\sqrt{3} \sin \phi_{cs}}{\sqrt{3} \cos \theta + \sin \theta \sin \phi_{cs}} \quad (8)$$

where, $p_0 =$ value of p' at the intersection of current swelling line with virgin consolidation line and ϕ_{cs} is critical state angle of shearing resistance. The projection of these curves on $J - p'$ plane is shown in Figure 1 where M_J is the slope of the critical state line (CSL).

Model specific variables (C_1 , C_2 , C_3) of flow vector for modified cam clay model can be computed as below.

$$C_1 = \frac{\partial F}{\partial p'} = \frac{1}{p'} \left[2 - \frac{p_0}{p'} \right] ; \quad C_2 = \frac{\partial F}{\partial J} = 2J \left(\frac{1}{p' g(\theta)} \right)^2 \quad (9)$$

$$C_3 = \frac{\partial F}{\partial \theta} = -2 \left(\frac{J}{p' g(\theta)} \right)^2 \frac{1}{g(\theta)} \frac{\sqrt{3} \sin \phi_{cs} (\sqrt{3} \sin \theta - \cos \theta \sin \phi_{cs})}{(\sqrt{3} \cos \theta + \sin \theta \sin \phi_{cs})^2}$$

Hardening/softening is controlled by parameter p_0 which is related to plastic volumetric strain. Increments in the yield surface dp_0 and hardening parameter A are given by the following equations.

$$d p_0 = \frac{v p_0}{\lambda - \kappa} d \varepsilon_v^p \quad \text{and} \quad A = -\frac{1}{\Lambda} \frac{\partial F}{\partial p'} d p_0 = \frac{p_0}{p_0} \frac{v}{\lambda - \kappa} C_1 \quad (10)$$

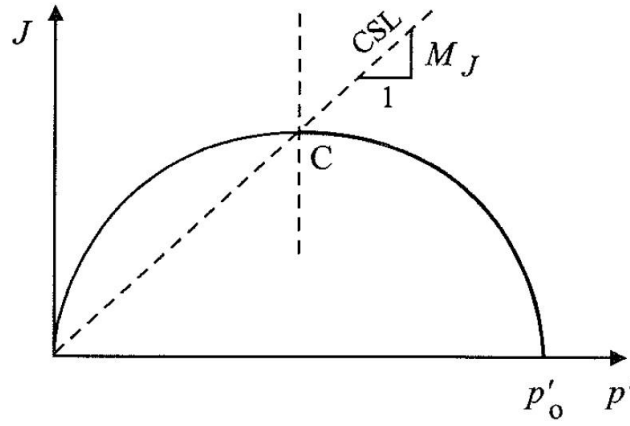


Figure 1 Projection of yield surface of modified Cam clay model on $J - p'$ plane

2.3. Nonlinear Algorithm

The static load is divided in ten equal parts and each part is applied separately and steps given below are followed for each part. The stiffness matrix, $[K]$ is maintained constant throughout the process. The algorithm to be used after application of each one tenth of load for nonlinear analysis is given below.

1. For first cycle of each equal part, apply one tenth value of total load as incremental load $\{\Delta F\}$. For next cycles, apply $\{\Delta F\}$ obtained in step (6) as incremental load. Following equation is solved to obtain incremental displacement, $\{\Delta u\} = [K]^{-1} \{\Delta F\}$.
2. Incremental displacement, Δq , is to be added to displacement obtained in previous increment u_{i-1} and displacement for i^{th} increment is obtained as $\{q\}_i = \{q\}_{i-1} + \{\Delta q\}$
3. The value of number of yielded elements, y_e , is set to be equal to zero.
4. The value of number of yielded points, y_p , is set to be equal to zero for each element.
5. From global incremental displacement vector Δu , elemental incremental displacement vector, $\{\Delta \delta\}$ is to be selected.
6. The incremental stress, $\{\Delta \sigma\}$ and total stress for i^{th} increment, $\{\sigma_i\}$, for all 27 Gauss points are obtained using relations given below:

$$\{\Delta \sigma\} = [D] [B] \{\Delta \delta\} \text{ and } \{\sigma_i\} = \{\sigma_{i-1}\} + \{\Delta \sigma\}$$

where, $\{\sigma_{i-1}\}$ is the total stress at $i-1^{\text{th}}$ iteration. $\{\sigma_i\}$ is checked with yield stress. If Gauss point under consideration is not yielded, next Gauss point is considered. Otherwise y_p is set equal to y_p+1 . Excess stress than the yield stress $\{\Delta \sigma\}_{\text{extra}}$ is calculated using following relation:

$$\{\Delta \sigma\}_{\text{extra}} = [D - D_{\text{ep}}] \{\Delta \varepsilon\}$$

The total stress is kept at yield level by the following equation,

$$\{\sigma_i\} = \{\sigma_i\} - \{\Delta \sigma\}_{\text{extra}}$$

The additional load vector $\{\Delta F\}$ is obtained as below to be applied in next iteration.

$$\{\Delta F\}^e = \iiint_V [B]^T \cdot \{\Delta \sigma\}_{\text{ext}} dV$$

Compute increment in the yield surface dp_0 and hardening parameter A .

This procedure is repeated for all Gauss points of the element.

If $y_p > 0$, y_e is set equal to $y_e + 1$.

Step (4) to (6) is repeated for all the elements.

7. If $y_e = 0$, it means that no element is yielded and next one tenth part of load is applied.
8. If $y_e > 0$, then convergence is checked using following criteria:

$$e_d = \left(\sqrt{\sum (q_i)^2} - \sqrt{\sum (q_{i-1})^2} \right) / \sqrt{\sum (q_i)^2}$$

where, e_d = displacement norm, q_i and q_{i-1} are total displacement at the i^{th} and $i-1^{\text{th}}$ iteration.

9. If the convergence criterion is observed, then next one tenth of load is applied. Else procedure from step (1) to step (9) is repeated till the convergence of the displacements.

3.0 VALIDATION

An experimental study was carried out by Prakash [26] on a laterally loaded pile embedded in sand. The section of the pile was hollow circular with diameter of 1.6 inch. In numerical modelling, it is converted into equivalent solid circular section. The equivalent modulus of elasticity of sand is calculated using the relation $E = J\gamma z$ [27], where z is the depth from the surface, γ is the density of soil and J is the dimensionless parameter whose value is taken as 350. The Poisson's ratio and unit weight of the sand are 0.25 and 18.9 kN/m³ respectively. The boundary below the tip was considered rigid and rough and the lateral boundary was considered rigid and smooth. The gapping between the pile and soil was prohibited but slipping was allowed. The displacements and variation of bending moment obtained experimentally by Prakash [26] and proposed software are compared and presented in Figure 2a and 2b. Maximum deviation obtained is 10% in displacements and 8% in bending moments. The results show reasonable agreement.

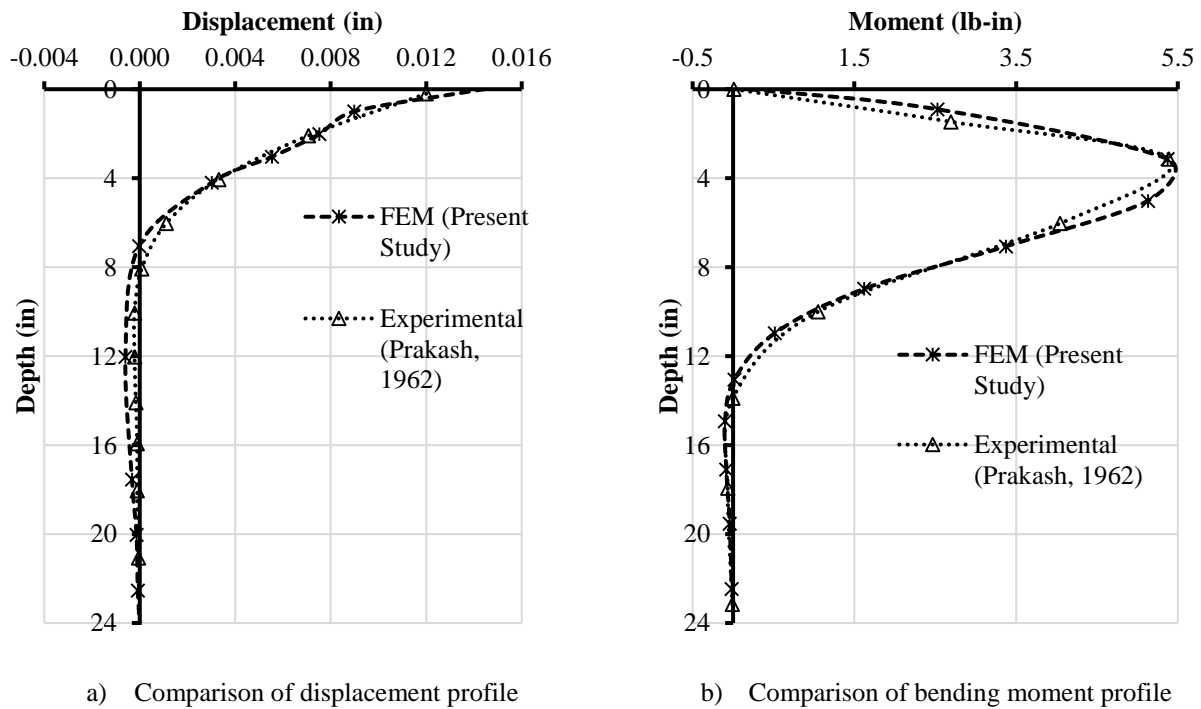


Figure 2 Validation with experimental result from Prakash (1962)

Comparison with pile load test data reported by Ismael and Klym [28] at Ontario is presented in Figure 3. A concrete pile with diameter 60 in (1.52m) was embedded in over-consolidated clay with cohesion 2000 lb/ft² (96.0 kPa).

Total pile length was 39 ft (12.0 m) with one foot (0.30 m) length above ground-line. The flexural rigidity EI of pile was 93×10^{10} lb-in² (2.675×10^6 kN.m²). Comparison between measured and predicted pile response shows a good agreement at higher load levels.

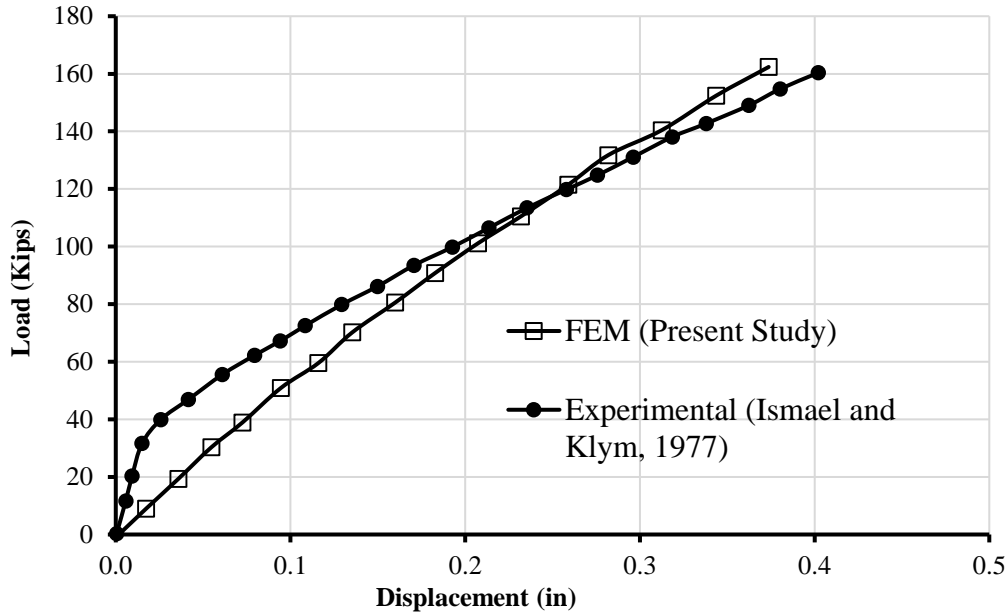


Figure 3 Validation with Experimental results (Ismael and Klym, 1977)

4.0 PARAMETRIC STUDY

A square pile group of 3×3 configuration (Figure 4) is subjected to lateral load of 2500 kN and is analyzed using parameters mentioned in Table 1. The effect of influencing parameters like soil modulus, pile spacing, pile diameter and pile slenderness is investigated. Load is applied in the increments of 50 kN. During each increment, the stress in the soil elements is calculated using elastic constitutive relation. It is compared to yield stress predicted by modified Cam clay criterion. If the stress produced is more than yield stress, the extra stress is converted into load and applied again. The process is repeated till the convergence in two successive values of the displacements is observed. Then next increment of load is applied. The displacement of the center of gravity of pile group at each load level is obtained and plotted as load-displacement graph for each case. In most cases, design of laterally loaded pile is governed by displacement criterion. Different codes suggest the displacement criteria to indicated ultimate load as 5 mm [29], 10% of diameter [30] and 20% of diameter [31]. Hence the loads at displacement of 5 mm, 10% of pile diameter and 20% of pile diameter are also obtained. The effect of parameter on maximum bending moment generated in the pile group is also studied.

To decide the optimum extent of the soil elements in model a mesh convergence study was carried out for typical case ($E_s = 30$ MPa, $s/D = 3$, $D = 1.0$ m, $L/D = 25$). It was observed that if soil is modeled beyond a distance of 14 times diameter from the pile surface, the change in the obtained results was negligible. Hence, for all cases the soil was modeled up to a distance of $14D$ from pile surface in all directions.

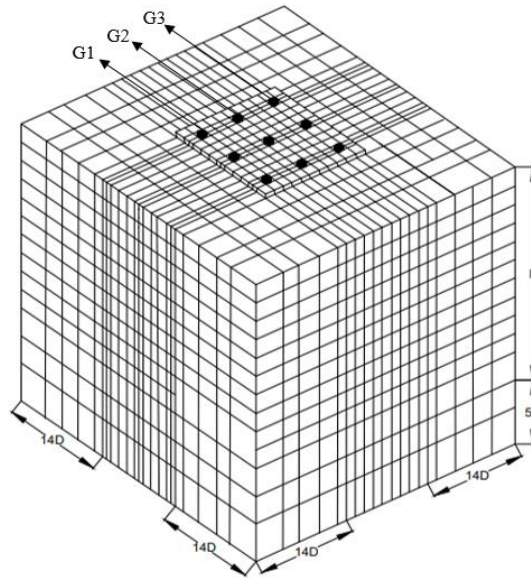


Figure 4 FEM mesh used for 3×3 square pile group configuration

Table 1 Properties of pile and soil used for parametric study

Soil properties	Value
Elasticity Modulus, E_s (MPa)	10 - 40
Unit Weight, γ_s (kN/m ³)	18.5
Poisson's ratio, μ_s	0.35
Cohesion, c (kPa)	110
Angle of internal friction, ϕ	0
Gradient of compression line, λ	0.14
Gradient of swelling line, κ	0.03
Specific volume, v	2.1
p' at the intersection of virgin consolidation line, p_0	60
Pile properties	
Elasticity Modulus, E_p (GPa)	25
Pile diameter, D (m)	0.7 to 1.0
Poisson's ratio, μ_p	0.25
L/D ratio	10, 15, 20 and 25
Unit Weight, γ_p (25 kN/m ³)	
s/D ratio	2, 3, 4 and 5
Thickness of Pile cap, t_p	0.55 m
Interface element	
Normal stiffness, K_n (kN/m ³)	1.0×10^7
Tangential stiffness, K_s (kN/m ³)	1100

4.1. Effect of Yield Criteria

Figure 5 shows the variation of the lateral displacement with applied load using Mohr- Coulomb (MC) and modified Cam clay (MCC) criterion for $E = 30 \text{ MPa}$, $s/D = 3$, $D = 1.0 \text{ m}$, $L/D = 25$. It is observed that modified Cam clay criterion overpredicts the displacements at all load levels. At maximum load the displacement is overpredicted by 43.15%. The ultimate load at displacement of 5 mm, 10% of diameter and 20% of diameter are underpredicted by 20.3%, 21.6% and 17.15% respectively. This may be attributed to yield surface parameter p_0 . MC model is Elastic-perfectly plastic. So up to initial yield it will bear more stiffness as compared to MCC model. MCC model depends on stress ratio p/p_0 . It is nonlinear from small strain levels as compared to MC model. The displacements at maximum load and ultimate loads predicted at displacement of 5 mm, 10% of diameter and 20% of diameter by both criteria are summarized in Table 2 and Table 3 for comparison.

Table 2 Comparison of displacement for different yield criteria

Yield Criteria	Displacement (mm)
Mohr-Coulomb	182.79
Modified Cam clay	261.68

Table 3 Ultimate loads predicted for different yield criteria

Failure Criterion	Mohr Coulomb	Modified Cam clay
P_u at $y = 5 \text{ mm}$ (kN)	410.50	327.17
P_u at $y = 0.1D$ (kN)	1882	1475.62
P_u at $y = 0.2D$ (kN)	2606.27	2159.24

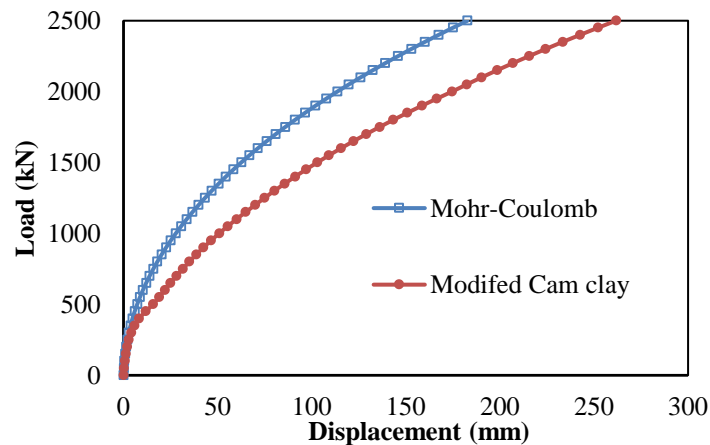


Figure 5 Load-displacement comparison for different yield criteria

4.2. Effect of Soil Modulus

Effect of soil modulus is investigated using modified Cam clay (MCC) criterion for values of soil modulus between 10 MPa to 40 MPa with the increment of 10 MPa and plotted in Figure 6. The common parameters are $s/D = 3$, $D = 1.0 \text{ m}$, $L/D = 25$. It is observed that the displacement of the pile group reduces with increase in soil modulus. When soil modulus is increased from 10000 MPa to 40000 MPa, at highest load of 2250 kN, the decrease in displacement is 64.31% whereas the decrease in bending moment is 27.01%. The effect of soil modulus on maximum bending moment generated in pile group is depicted in Figure 7. The ultimate loads predicted at displacement of 5 mm, 10% of diameter and 20% of diameter increase by 70.45%, 68.76% and 69.73%

respectively. This is due to increase in soil stiffness. The displacements and maximum bending moments generated for different soil modulus are mentioned in Table 4. The ultimate loads predicted at displacement of 5 mm, 10% of diameter and 20% of diameter at different soil modulus are summarized in Table 5 for comparison.

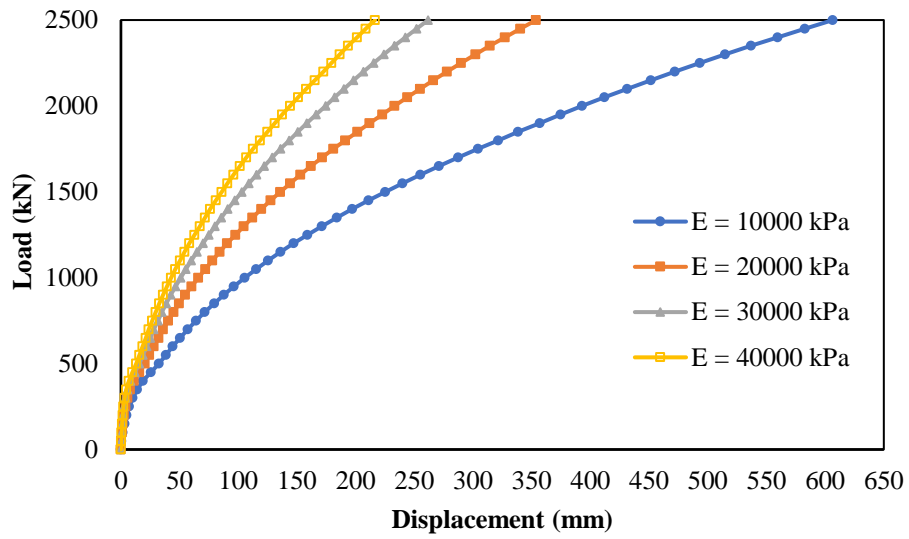


Figure 6 Load-displacement comparison for different soil modulus using MCC criteria

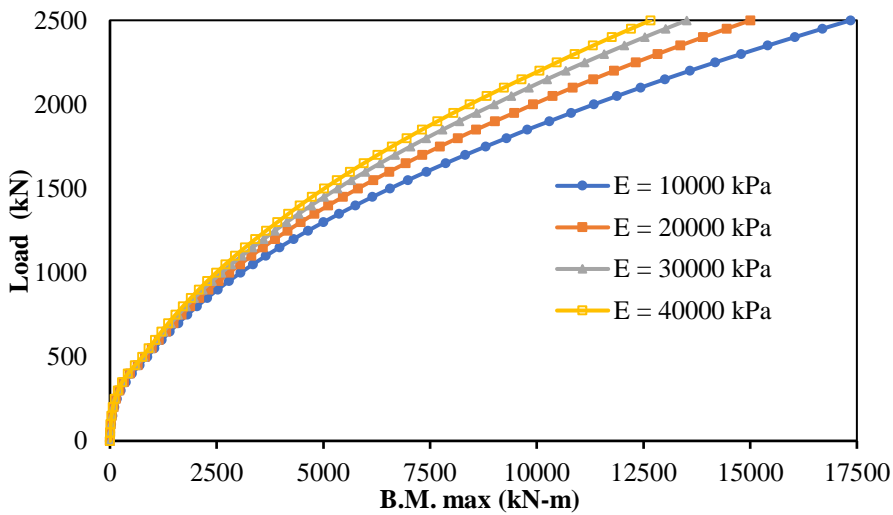


Figure 7 Load-maximum bending moment comparison for different soil modulus using MCC criteria

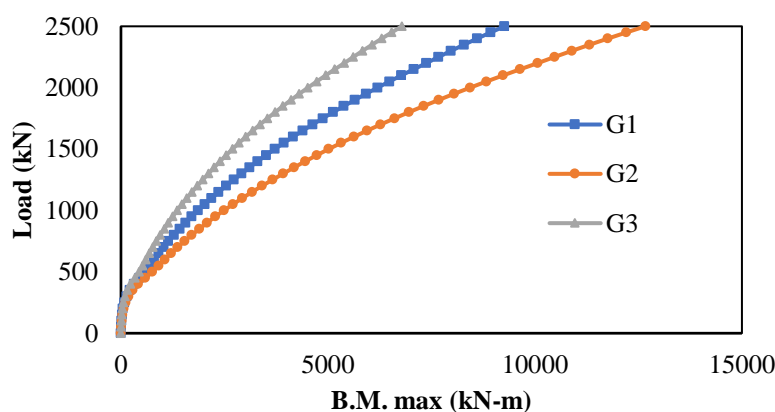
Table 4 Comparison of displacement and maximum bending moment for different soil modulus

Parameter	$E = 10000$ kPa	$E = 20000$ kPa	$E = 30000$ kPa	$E = 40000$ kPa
Displacement (mm)	606.64	353.82	261.68	216.49
B.M.max (kN-m)	17356.28	17356.28	13516.95	12668.34

Table 5 Ultimate loads predicted for different soil modulus

Failure Criterion	$E = 10000 \text{ kPa}$	$E = 20000 \text{ kPa}$	$E = 30000 \text{ kPa}$	$E = 40000 \text{ kPa}$
P_u at $y = 5 \text{ mm}$ (kN)	209.44	280.23	327.17	357.58
P_u at $y = 0.1D$ (kN)	969.87	1266.39	1476.63	1636.76
P_u at $y = 0.2D$ (kN)	1410.09	1842.07	2159.24	2393.4

Bending moment generated in three rows of a pile group are calculated at each load level. It is observed that bending moment generated in middle row is highest for all cases considered in this study. A typical comparison of maximum bending moments generated in piles in front row (G1), middle row (G2) and rear row (G3) for $E = 40 \text{ MPa}$ is presented in Figure 8.

**Figure 8** Load-maximum B.M. comparison for piles in different rows at $E = 40 \text{ MPa}$ using MCC criteria

4.3. Effect of pile spacing

Pile spacing to diameter (s/D) ratio is changed from 2 to 5 with increment of one and its effect is investigated using modified Cam clay model and plotted in Figure 9 and Figure 10 for lateral displacement and maximum bending moment respectively. The common parameters are $E_s = 30 \text{ MPa}$, $D = 1.0 \text{ m}$, $L/D = 25$. As s/D ratio is increased, the reduction in displacement at all load levels is observed. This is because when spacing between the pile is increased keeping the number of piles constant, more soil available between the piles is mobilized in lateral direction. Also, the overlapping of pressure zone is less. When s/D ratio is increased from 2 to 5, at highest load of 2250 kN, the decrease in displacement of 42.44% is observed. The ultimate loads predicted at displacement of 5 mm, 10% of diameter and 20% of diameter increase by 36.47%, 38.56% and 36.26% respectively. The maximum bending moments generated increases by 22.79%. The displacements and maximum bending moments generated at maximum load are mentioned in Table 6. The ultimate loads predicted at displacement of 5 mm, 10% of diameter and 20% of diameter at different s/D ratio are summarized in Table 7 for comparison.

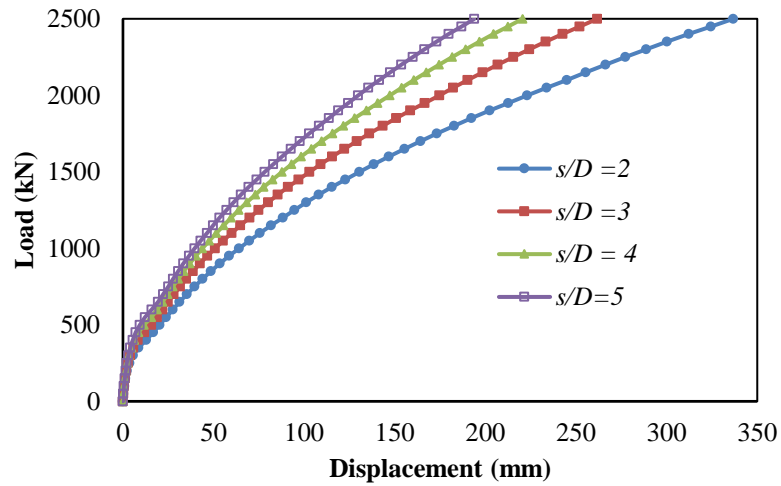


Figure 9 Load-displacement comparison for different pile spacing using MCC criteria

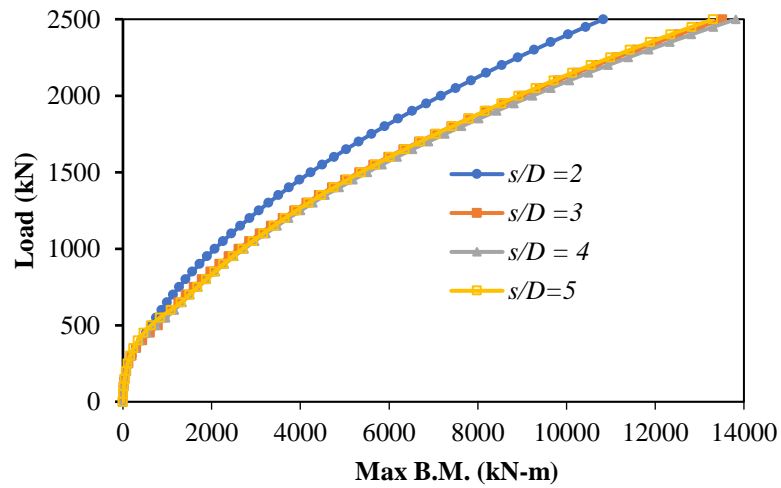


Figure 10 Load-maximum bending moment comparison for different pile spacing using MCC criteria

Table 6 Comparison of displacement and maximum bending moment for different pile spacing

Parameter	$s/D = 2$	$s/D = 3$	$s/D = 4$	$s/D = 5$
Displacement (mm)	336.85	261.78	220.55	193.91
B.M. max (kN-m)	10834.08	13516.95	13816.51	13303.74

Table 7 Ultimate loads predicted for different pile spacing

Failure Criterion	$s/D = 2$	$s/D = 3$	$s/D = 4$	$s/D = 5$
P_u at $y = 5$ mm (kN)	283.25	327.17	360.35	386.57
P_u at $y = 0.1D$ (kN)	1290.51	1475.63	1614.12	1707.13
P_u at $y = 0.2D$ (kN)	1887.57	2150	2373.65	2542.01

4.4. Effect of pile diameter

This influence is investigated by changing the pile diameter from 0.7 m to 1 m. The default parameters are $E_s = 30$ MPa, $s/D = 3$, $L/D = 25$. Modified Cam clay model is used and the results are plotted in Figure 11 and Figure 12 for lateral displacement and maximum bending moment respectively. The reduction in displacement with increase in pile diameter is observed. As the diameter is increased, more soil is mobilized in lateral direction causing increase in passive resistance. This reduces the displacement and increases the lateral load carrying capacity. If the diameter is increased from 0.7 to 1 m, the displacement is reduced by 33.38%. The ultimate loads predicted at displacement of 5 mm, 10% of diameter and 20% of diameter increase by 29.39%, 51.49% and 49.37% respectively. The maximum bending moment increases by 95.45%. The displacements and maximum bending moments generated at maximum load are mentioned in Table 8. The ultimate loads predicted at displacement of 5 mm, 10% of diameter and 20% of diameter at different pile diameter (D) are summarized in Table 9.

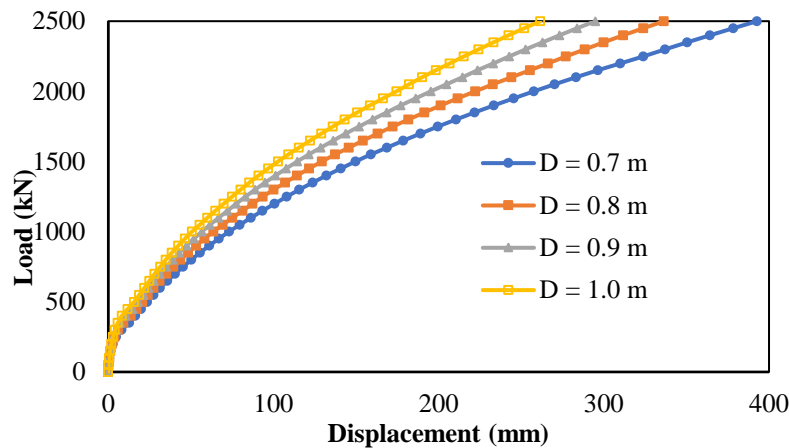


Figure 11 Load-displacement comparison for different pile diameter using MCC criteria

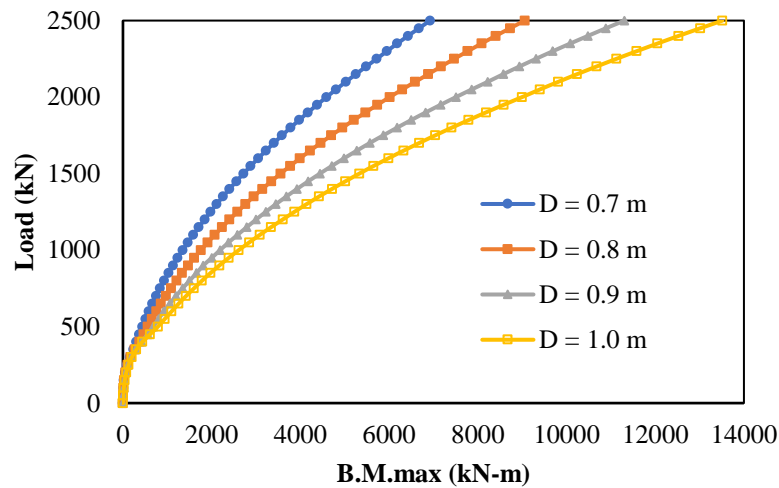


Figure 12 Load-maximum bending moment comparison for different pile diameter using MCC criteria

Table 8 Comparison of displacement and maximum bending moment for different pile diameter

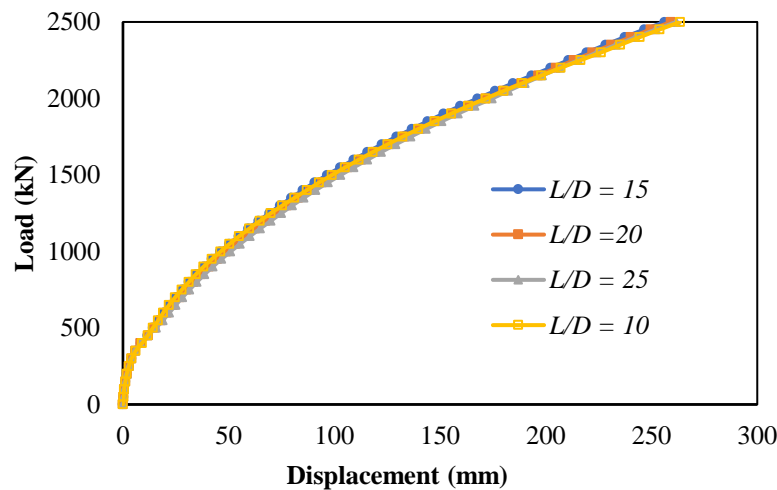
Parameter	$D = 0.7$ m	$D = 0.8$ m	$D = 0.9$ m	$D = 1.0$ m
Displacement (mm)	392.83	336.43	294.84	261.68
B.M. max (kN-m)	6926.18	9060.97	11306.76	13516.95

Table 9 Ultimate loads predicted for different pile diameter

Failure Criterion	$D = 0.7 \text{ m}$	$D = 0.8 \text{ m}$	$D = 0.9 \text{ m}$	$D = 1.0 \text{ m}$
P_u at $y = 5 \text{ mm}$ (kN)	252.85	278.4	304.57	327.17
P_u at $y = 0.1D$ (kN)	974.06	1139.49	1305.22	1475.63
P_u at $y = 0.2D$ (kN)	1445.56	1682.35	1915.62	2159.24

4.5. Effect of L/D ratio

Effect of pile slenderness is investigated by changing the length to diameter (L/D) ratio of pile from 10 to 25 with the increment of 5. As L/D ratio is increased, pile slenderness is increased and it causes increase in displacement of the pile. In contrary, increase in L/D ratio also causes passive resistance of the soil acting on more length of the pile. This reduces the pile displacement. The final influence of increase in L/D ratio is the algebraic sum of the contradictory effects due to these two phenomena. In the present study, with common parameters as $E_s = 30000 \text{ kPa}$, $s/D = 3$, $D = 1.0 \text{ m}$ and use of modified Cam clay model, very small change (0.60%) in displacement is observed at highest load (Figure 13). However, the maximum bending moment reduces by 27.68% (Figure 14). The ultimate load at displacement of 5 mm is found to be increasing consistently, as L/D ratio is increased from 10 to 25. However, ultimate loads at displacement of 10% of diameter and 20% of diameter increase as L/D ratio changes from 10 to 15 and after that decrease consistently up to L/D ratio of 25. The displacements and maximum bending moments generated at maximum load are mentioned in Table 10. The ultimate loads predicted at displacement of 5 mm, 10% of diameter and 20% of diameter at different s/D ratio are summarized in Table 11 for comparison.

**Figure 13** Load-displacement comparison for different L/D ratio using MCC criteria

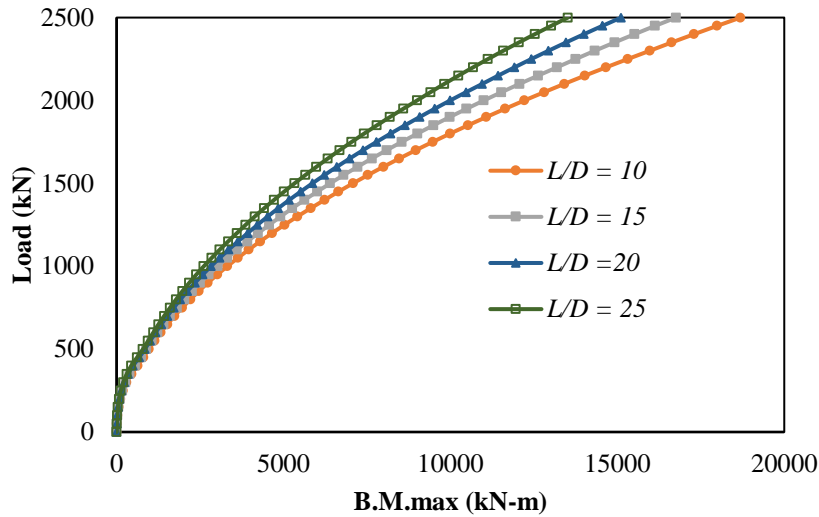


Figure 14 Load-maximum bending moment comparison for different L/D ratio using MCC criteria

Table 10 Comparison of displacement and maximum bending moment for different L/D ratio

Parameter	$L/D = 10$	$L/D = 15$	$L/D = 20$	$L/D = 25$
Displacement (mm)	263.56	256.15	259.23	261.68
B.M.max (kN-m)	18691.7	16758.57	15111.61	13516.95

Table 11 Ultimate loads predicted for different L/D ratio

Failure Criterion	$L/D = 10$	$L/D = 15$	$L/D = 20$	$L/D = 25$
P_u at $y = 5$ mm (kN)	322.54	326.4	326.57	327.17
P_u at $y = 0.1D$ (kN)	1509.92	1527.37	1498.66	1475.62
P_u at $y = 0.2D$ (kN)	2161.36	2187.01	2175.06	2159.24

5.0 CONCLUSIONS

After the analysis of the 3×3 pile group subjected to a lateral load of 2250 kN, with soil behavior represented by modified Cam clay criterion, the following conclusions are drawn.

1. Modified Cam clay criterion overpredicts the displacement by 43.15% more than the Mohr-Coulomb criterion. The ultimate loads at a displacement of 5 mm, 10% of pile diameter and 20% of pile diameter are underpredicted by 20.3%, 21.6% and 17.15% respectively. This may be attributed to the yield surface parameter p_0 .
2. When the elastic modulus of soil increases from 10000 kPa to 40000 kPa, the pile displacement decreases by 64.31% and the maximum bending moment reduces by 27.01% using the modified Cam clay criterion. The ultimate loads predicted at a displacement of 5 mm, 10% of diameter and 20% of diameter increase by 70.45%, 68.76% and 69.73% respectively. This is due to an increase in soil stiffness which allows less yielding of soil.
3. When the s/D ratio increases from 2 to 5, the decrease in pile displacement is by 42.44% and the maximum bending moment increases by 22.79% using the modified Mohr-Coulomb criterion. The ultimate loads predicted at a displacement of 5 mm, 10% of diameter and 20% of diameter increase by 36.47%, 38.56% and 36.26% respectively. This is due to the lesser overlapping of pressure zones and higher availability of passive resistance at higher pile spacing.
4. As the pile diameter increases from 0.7 m to 1.0 m, the pile displacement reduces by 33.38% and the maximum bending moment increases by 95.45% using the modified Cam clay criterion. The ultimate loads predicted at

a displacement of 5 mm, 10% of diameter and 20% of diameter increase by 29.39%, 51.49% and 49.37% respectively. This may be attributed to the higher mobilisation of passive resistance of soil by higher pile diameter.

5. As the L/D ratio increases from 10 to 25, the reduction in pile displacement is very small (0.60%) and the maximum bending moment is reduced by 27.68% using the modified Cam clay criterion. The ultimate load at a displacement of 5 mm is found to be increasing consistently, as the L/D ratio is increased from 10 to 25. However, ultimate loads at a displacement of 10 % of diameter and 20% of diameter increase as the L/D ratio changes from 10 to 15 and after that decreases consistently up to the L/D ratio of 25.

Conflicts of Interest

The authors have no competing interest to declare that is relevant to the content of this article.

Acknowledgement

There is no funding information supporting this study.

References

- [1] Reese, L. C. (1965). Non-dimensional solution for laterally loaded piles with soil modulus assumed proportional to depth. In Proc. 8th Texas Conf. SMFE. The Univ. of Texas.
- [2] Broms, B. B. (1964). Lateral resistance of piles in cohesionless soils. Journal of the soil mechanics and foundations division, 90(3), 123–156.
- [3] Sogge, R. L. (1981). Laterally loaded pile design. Journal of the Geotechnical Engineering Division, 107(9), 1179–1199.
- [4] Rajashree, S. S., & Sundaravadivelu, R. (1996). Degradation model for one-way cyclic lateral load on piles in soft clay. Computers and Geotechnics, 19(4), 289–300. [https://doi.org/10.1016/S0266-352X\(96\)00008-0](https://doi.org/10.1016/S0266-352X(96)00008-0)
- [5] Desai, C. S., & Appel, G. C. (1976). 3-D analysis of laterally loaded structures. In Proceedings of the 2nd international conference on numerical methods in geomechanics, Blacksburg (pp. 405–418).
- [6] Yegian, M., & Wright, S. G. (1973). Lateral Soil Resistance Displacement Relationships for Pile Foundation in Soft clays. In Offshore Technology Conference. Offshore Technology Conference. <https://doi.org/10.4043/1893-MS>
- [7] Baguelin, F., & Frank, R. (1980). Theoretical studies of piles using the finite element method. In Numerical methods in offshore piling (pp. 83–91). Thomas Telford Publishing.
- [8] Randolph, M. F. (1981). The response of flexible piles to lateral loading. Géotechnique, 31(2), 247–259. <https://doi.org/10.1680/geot.1981.31.2.247>
- [9] Al-Khazaali, M., & Vanapalli, S. K. (2015). Numerical modelling technique to predict the load versus settlement behavior of single piles in unsaturated coarse-grained soils. Proc. of GeoQuébec. <https://doi.org/10.13140/RG.2.1.3500.0081>
- [10] al-Damluji, O. al-F. S., & Al-Anbaki, U. S. (2010). Three-Dimensional Finite Element Analyses of a Single Pile in an Elastoplastic Clayey Soil. Journal of Engineering, 16(3).
- [11] Desai, C. S., Alameddine, A. R., & Kuppusamy, T. (1981). Pile cap-pile group-soil interaction. Journal of the Structural Division, 107(5), 817–834.
- [12] Desai, C. S., & Abel, J. F. (1971). Introduction to the finite element method; a numerical method for engineering analysis. Van Nostrand Reinhold.
- [13] Zaman, M. M., Najjar, Y. M., & Muqtadir, A. (1993). Effects of cap thickness and pile inclination on the response of a pile group foundation by a three-dimensional nonlinear finite element analysis. Computers and Geotechnics, 15(2), 65–86. [https://doi.org/10.1016/0266-352X\(93\)90018-3](https://doi.org/10.1016/0266-352X(93)90018-3)
- [14] Hazzar, L., Karray, M., Bouassida, M., & Hussien, M. N. (2013). Ultimate Lateral Resistance of Piles in Cohesive Soil. DFI Journal - The Journal of the Deep Foundations Institute, 7(1), 59–68. <https://doi.org/10.1179/dfi.2013.005>
- [15] Ilyas, T., Leung, C. F., Chow, Y. K., & Budi, S. S. (2004). Centrifuge Model Study of Laterally Loaded Pile Groups in Clay. Journal of Geotechnical and Geoenvironmental Engineering, 130(3), 274–283. [https://doi.org/10.1061/\(ASCE\)1090-0241\(2004\)130:3\(274\)](https://doi.org/10.1061/(ASCE)1090-0241(2004)130:3(274))
- [16] Chandrasekaran, S. S., Boominathan, A., & Dodagoudar, G. R. (2010). Experimental Investigations on the Behaviour of Pile Groups in Clay Under Lateral Cyclic Loading. Geotechnical and Geological Engineering, 28(5), 603–617. <https://doi.org/10.1007/s10706-010-9318-4>
- [17] Dewaikar, D. M., Verghese, S., Sawant, V. A., & Chore, H. S. (2007). Non-linear 3-D FEA of laterally loaded pile group incorporating no-tension behaviour of soil. Indian Geotech. J, 37(3), 174–189.

- [18] Karthigeyan, S., Ramakrishna, V. V. G. S. T., & Rajagopal, K. (2007). Numerical Investigation of the Effect of Vertical Load on the Lateral Response of Piles. *Journal of Geotechnical and Geoenvironmental Engineering*, 133(5), 512–521. [https://doi.org/10.1061/\(ASCE\)1090-0241\(2007\)133:5\(512\)](https://doi.org/10.1061/(ASCE)1090-0241(2007)133:5(512))
- [19] Abu-Farsakh, M., Sourì, A., Voyiadjis, G., & Rosti, F. (2018). Comparison of static lateral behavior of three pile group configurations using three-dimensional finite element modeling. *Canadian Geotechnical Journal*, 55(1), 107–118. <https://doi.org/10.1139/cgj-2017-0077>
- [20] Halder, A., & Bandyopadhyay, K. (2016). Lateral Load Carrying Capacity Of Piles In Layered Cohesive Soil. In *Indian Geotechnical Conference IGC2016* (pp. 15–17).
- [21] Yu, Y., Shen, M., & Hsein Juang, C. (2019). Assessing Initial Stiffness Models for Laterally Loaded Piles in Undrained Clay: Robust Design Perspective. *Journal of Geotechnical and Geoenvironmental Engineering*, 145(10), 04019073. [https://doi.org/10.1061/\(ASCE\)GT.1943-5606.0002074](https://doi.org/10.1061/(ASCE)GT.1943-5606.0002074)
- [22] Li, X.-Y., Wan, J.-H., Zhao, H.-P., & Liu, S.-W. (2021). Three-Dimensional Analysis of Nonlinear Pile–Soil Interaction Responses Using 3D Pile Element Model. *International Journal of Geomechanics*, 21(8), 04021129. [https://doi.org/10.1061/\(ASCE\)GM.1943-5622.0002076](https://doi.org/10.1061/(ASCE)GM.1943-5622.0002076)
- [23] Luo, R., Zhu, B., & Yang, Z. (2021). Limiting Force Profile for Laterally Loaded Piles in Undrained Clay. *International Journal of Geomechanics*, 21(8), 04021146. [https://doi.org/10.1061/\(ASCE\)GM.1943-5622.0002066](https://doi.org/10.1061/(ASCE)GM.1943-5622.0002066)
- [24] Potts, D. M., Zdravković, L., Addenbrooke, T. I., Higgins, K. G., & Kovačević, N. (2001). *Finite element analysis in geotechnical engineering: application (Vol. 2)*. Thomas Telford London.
- [25] Nayak, G. C., & Zienkiewicz, O. C. (1972). Convenient Form of Stress Invariants for Plasticity. *Journal of the Structural Division*, 98(4), 949–954. <https://doi.org/10.1061/JSDEAG.0003219>
- [26] Prakash, S. (1962). *Behavior of pile groups subjected to lateral loads*. University of Illinois at Urbana-Champaign.
- [27] Terzaghi, K., Peck, R. B., & Mesri, G. (1996). *Soil mechanics in engineering practice*. John Wiley & sons.
- [28] Ismael, N. F., & Klym, T. W. (1978). Behavior of Rigid Piers in Layered Cohesive Soils. *Journal of the Geotechnical Engineering Division*, 104(8), 1061–1074. <https://doi.org/10.1061/AJGEB6.0000678>
- [29] Standard, I. (1985). *Indian standard code of practice for design and construction of pile foundations, part 4: load test on piles*. IS.
- [30] Congress, I. R. (2016). *Standard specifications and code of practice for road bridges*. In *Indian Roads Congress* (pp. 1–89).
- [31] Rao, S. N., Ramakrishna, V. G. S. T., & Rao, M. B. (1998). Influence of Rigidity on Laterally Loaded Pile Groups in Marine Clay. *Journal of Geotechnical and Geoenvironmental Engineering*, 124(6), 542–549. [https://doi.org/10.1061/\(ASCE\)1090-0241\(1998\)124:6\(542\)](https://doi.org/10.1061/(ASCE)1090-0241(1998)124:6(542))